SUGISAKA MASANORI

Journal of Robotics, Networking and Artificial Life
Vol. 10(1); June (2023), pp. 25–32
ISSN (Online): 2352-6386; ISSN (Print): 2405-9021
https://alife-robotics.org/jrnal.html

Research Article

Forward Kinematic of a Sphere Considering Slipping and Motion Analysis in Three Rollers

Kenji Kimura[1], Koki Ogata[2], Hiroyasu Hirai[3], Takumi Ueda[3], Kazuo Ishii[3]
[1]*Department of Control Engineering, National Institute of Technology, Matsue College, 14-4 Nishi-ikuma-cho, Matsue-shi, Shimane,690-8518, Japan*
[2]*DENSO, 2-1, Nagane, Sato-cho, Anjo-shi, 446-8511, Aichi, Japan*
[3]*Graduate School of Life Science and Engineering, Kyushu Institute of Technology, 2-4 Hibikino, Wakamatsu-ku, Kitakyushu-shi 808-0196, Fukuoka, Japan*

ARTICLE INFO

Article History

Received 24 November 2022
Accepted 17 August 2023

Keywords
Angular velocity vector of the sphere
Motion analysis of the sphere
Slip velocity vector of the sphere

ABSTRACT

Compared to mobile robots equipped with multiple rollers, spherical robots can move in all directions and are superior in durability and in their ability to climb steps. Slippage between balls and rollers is a significant problem in friction drives. However, previously established roller-driven ball kinematics model considers sliding on only two constraining rollers. In this research, we developed it, proposed a motion model of sphere with three-constraint rollers, and developed a mathematical model that simulates the angular velocity vector of the sphere and the slip vector at each contact point. And we considered the existence of an angular velocity vector of sphere adapted three constraint rollers from the viewpoint of forward kinematics and succeed demonstration of the trajectory of the endpoint of the angular velocity vector and slip velocity vector of sphere.

1. Introduction

Spherical robots are widely used in robotics, such as multi-finger fingertip mechanism for hand robots, actuator transmission mechanisms for omnidirectional movement, and driving mobile robots. They are also used as driving rollers for omnidirectional movement mechanisms; there are various arrangements and spherical structures depending on the requirements of the movement mechanism. Figure 1 shows the roller contact type for the number of actuators ($\boldsymbol{N_R}$) per sphere.

In the case of $N_R = 2$, ACROBAT-S [1] (Figure 1(a)) and wheel chair [2] (Figure 1(b)) with sphere kinematics are developed for transportation service. The omnidirectional locomotion condition is that two rotational axes contact point with sphere are arranged along the great circle. Thus, the angular velocity vector of the sphere lies on a common plane parallel to the great circle of sphere. In this way, the roller arrangement conditions for omni directional spherical mobile robot are derived [3]. Furthermore, in this situation, the angular velocity vector of the sphere has two degrees of freedom. Using this theory, spherical robot transfer problem is considered in [4]-[7], as models don't consider slipping.

As shown in Figure 1(c), the examples of the ball-holding mechanism are Musashi150 [8], RV-infinity [9], and NuBot [10], which are designed to transport ball. Most teams in the RoboCupMSL(Middle-Size-League) adapts a ball-holding mechanism with two rollers on the upper hemisphere to control the rotational motion of the ball. In most developments, roller arrangement that causes slippage (when the roller rotational axis don't have slip in along a great circle) is adopted. Now there is slippage at contact point between the roller and the ball. It utilizes the ability to hold the ball due to frictional force. However, in the absence of a suitable mathematical model, the roller arrangement is heuristically determined experimentally.

In a previous study, we used two constraint rollers that allowed the slipping to derive a mathematical

Corresponding author's E-mail: k-kimura@matsue-ct.jp, koki.ogata.j4s@jp.denso.com, multipletitan@gmail.com, ishii@brain.kyutech.ac.jp

model for spherical rotational motion for forward kinematics [11]. This model is included in the kinematics of [3]. Furthermore, we employed experiment [12] to validate the model of [11].

In the case of $N_R = 3$, omnidirectional-wheeled mobile platform (OWMP) [13] has three-constraint rollers (Figure 1(d)), while a ball-balanced robot [14] has three unconstraint rollers (Figure 1(e)). In the example of an adapted unconstraint three rollers, ball-valanced robot can move in omni-direction [15]. Furthermore, it attempts to carry the load using couple of it ([15] and [16]). Ball valanced robot (Figure 1(e)) [14] has an adapted roller in the upper hemisphere, whereas Atras sphere [17] has an adapted roller in the lower hemisphere and can control sphere.

Although there are three rollers, the sphere rotational dimensions are different because of the roller structure (constraint type or unconstraint type). Each constrained roller has less rotational diversity than the unconstrained rollers. However, the holding force is stronger than that of the unconstrained roller. The stability of the sphere rotational motion is higher in the case of three rollers than in the case of two rollers. OWMP [13] is used kinematic with roller arrangement restricted to the equator; we extended this kinematics to an arbitrary roller's arrangement discussion.

In this study, we modified the previously developed kinematic model [11] for the case of three-constraint rollers. And presented a novel mathematical model

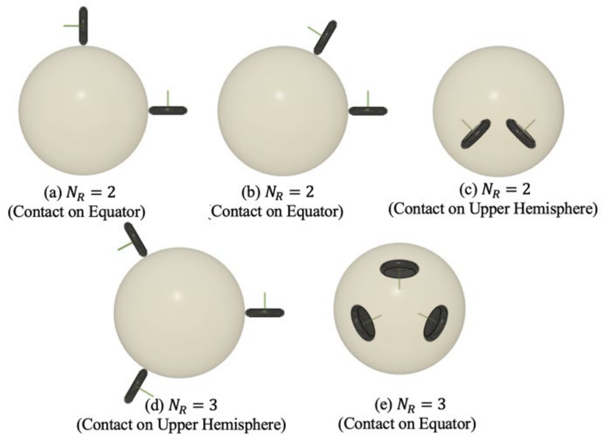

Figure 1. A pattern of roller arrangement for sphere mobile robot driven by multiple rollers.

about sphere rotational motion using three-constraint rollers that allows for slipping. Additionally, we simulate the angular velocity vector of the sphere, the sphere mobile speed vector, slip vector between the roller and the ball and the slip speed using forward kinematics.

The rest of this study is as follows: Chapter 2 discusses the existing space of angular velocity vectors on rollers and drives the sphere's kinematics with three rollers. Chapter 3 conducted the simulation. Finally, we present the summary and future works.

2. The sphere forward kinematics for three constraint rollers

In this chapter, we introduce the angular velocity vector of the sphere to model the sphere's rotational motion geometrically.

2.1 *Consideration of existence of angular velocity vector of the sphere*

(A) Case of single-constraint driving roller

Table 1 shows variables list for this study. Figure 2(a) shows existence space of angler velocity vector of sphere in a single-roller. The center $\boldsymbol{O}$ of a sphere with radius r is fixed as the origin of the coordinate system $\Sigma - xyz$. The constraint roller i have the center of gravity $\boldsymbol{R_i}$ and $\boldsymbol{q_i}$ denotes contact point between roller i and sphere. $\boldsymbol{\eta_i}$ denotes the unit vector along the rotational axis of the constraint roller. $\boldsymbol{O}$, $\boldsymbol{q_i}$ and $\boldsymbol{R_i}$ are arranged on common line. $\boldsymbol{\omega}$ denotes the angular velocity vector of the sphere. v_i denotes the peripheral speed of the constraint roller i at $\boldsymbol{q_i}$on sphere. $\boldsymbol{\mathcal{V}_i^S}(= \boldsymbol{\omega} \times \boldsymbol{q_i})$ denote the velocity vector of the sphere with respect to $\boldsymbol{q_i}$.

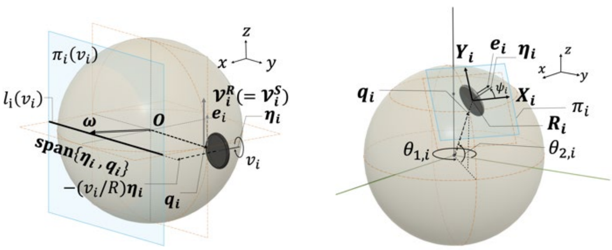

(a) (b)

Figure 2 (a) The existence of sphere angler velocity vector in the case of a single-constraint roller. (b) Roller's axis vector $\boldsymbol{\eta_i}$ at contact point $\boldsymbol{q_i}$ on the sphere

Table 1 Variables list

$\Sigma - xyz$	Three-dimensional coordinate system fixed the center of sphere
$\langle \boldsymbol{x}, \boldsymbol{y} \rangle$	Inner product with respect to $\boldsymbol{x}$ and $\boldsymbol{y}$
$\lVert \boldsymbol{x} \rVert$	Norm of vector $\boldsymbol{x}$
$\mathrm{span}\{\boldsymbol{x}, \boldsymbol{y}\}$	Plane spanned by $\boldsymbol{x}$ and $\boldsymbol{y}$
$\boldsymbol{O}$	Origin of $\Sigma - xyz$(Center of sphere)
$\boldsymbol{q}_i$	Contact point from sphere and roller
$\boldsymbol{\eta}_i$	Unit vector of constraint-roller along the rotational axis direction
$\boldsymbol{\omega}$	Sphere angular velocity vector
$\boldsymbol{R}_i$	Center of gravity of constraint roller
$\boldsymbol{v}_i^R$	Velocity vector of constraint roller i at $\boldsymbol{q}_i$
$\boldsymbol{v}_i^S$	Velocity vector of sphere at $\boldsymbol{q}_i$
$\zeta_{i,k}$	Slip velocity of the sphere with respect to $\boldsymbol{v}_i^R$ in k-th pattern of roller arrangement ($k = 1,2,3,4$)
$\boldsymbol{V}_k$	Sphere mobile speed in k-th pattern of roller arrangement ($k = 1,2,3,4$)
$\boldsymbol{\omega}_k$	Sphere angular velocity vector in k-th pattern of roller arrangement ($k = 1,2,3,4$)
$\boldsymbol{e}_i$	Unit normal vector along $\boldsymbol{v}_i^R$
$\boldsymbol{V}$	Sphere robot velocity vector on xy-plane
ψ_i	Roller arrangement angle that rotates counterclockwise with respect to
$l_i(v_i)$	Existence set of end point of $\boldsymbol{\omega}$ with respect to v_i
v_i	Peripheral speed of constraint roller i
r	Sphere robot radius
φ	Sphere robot direction
d_i	the minimal distances between point and line

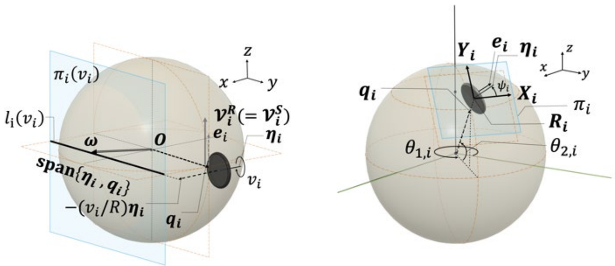

(a) (b)

Figure 2 (a) The existence of sphere angler velocity vector in the case of a single-constraint roller. (b) Roller's axis vector $\boldsymbol{\eta}_i$ at contact point $\boldsymbol{q}_i$ on the sphere

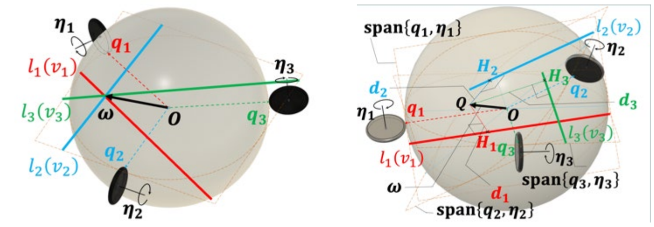

(a) (b)

Figure 3 Slip adjudication by the location $l_1(v_1)$, $l_2(v_2)$ and $l_3(v_3)$. (a). A pair $\{v_1, v_2, v_3\}$ exists such that $l_1(v_1)$, $l_2(v_2)$ and $l_3(v_3)$ have points in common. (b). A pair $\{v_1, v_2, v_3\}$ exists such that $l_1(v_1)$, $l_2(v_2)$ and $l_3(v_3)$ have no points in common.

$\boldsymbol{v}_i^R$ denotes velocity vector of the roller. $\boldsymbol{e}_i$ denotes unit normal vector along $\boldsymbol{v}_i^R$. Because of $\boldsymbol{e}_i \in \mathbf{span}\{\boldsymbol{q}_i, \boldsymbol{\eta}_i\}$, $\boldsymbol{e}_i$ and $\boldsymbol{v}_i^R$ are satisfy $v_i = \langle \boldsymbol{v}_i^R, \boldsymbol{e}_i \rangle$. Thus. Nonslip condition is $\boldsymbol{v}_i^S = \boldsymbol{v}_i^R$ and $\boldsymbol{\omega}$ can be satisfied as follow.

$$\boldsymbol{v}_i^S = \boldsymbol{\omega} \times \boldsymbol{q}_i \tag{1}$$

$\boldsymbol{e}_i \in \mathbf{span}\{\boldsymbol{q}_i, \boldsymbol{\eta}_i\}$ is the unit normal vector along $\boldsymbol{v}_i^R$. Using $v_i = \langle \boldsymbol{v}_i^R, \boldsymbol{e}_i \rangle$ ($\boldsymbol{v}_i^S = \boldsymbol{v}_i^R$: nonslip condition) and Eq. (1), v_i is represented as follows:

$$v_i = \langle \boldsymbol{v}_i^R, \boldsymbol{e}_i \rangle = -r\langle \boldsymbol{\eta}_i, \boldsymbol{\omega} \rangle \tag{2}$$

Thus, $\boldsymbol{\omega}$ can be satisfied as Eq. (3).

$$\langle \boldsymbol{\eta}_i, \boldsymbol{\omega} \rangle = -\frac{v_i}{r} \tag{3}$$

$\boldsymbol{\omega}$ must be on $\mathbf{span}\{\boldsymbol{\eta}_i, \boldsymbol{q}_i\}$ and can be represented as a following line set $l_i(v_i)$ that is parallel to $\boldsymbol{q}_i$ and passes through the end point of $-(v_i/r)\boldsymbol{\eta}_i$.

$$l_i(v_i) = \left\{ \boldsymbol{\omega} \middle| \left(-\frac{v_i}{r}\right)\boldsymbol{\eta}_i + t(1/r)\boldsymbol{q}_i, t \in \mathbb{R} \right\} \tag{4}$$

Furthermore, we set the roller contact point and rotational axis on the sphere. Contact point $\boldsymbol{q}_i$ is defined as a polar coordinate as follows:

$$\boldsymbol{q}_i = \left[\cos\theta_{2,i}\cos\theta_{1,i}, \cos\theta_{2,i}\sin\theta_{1,i}, \sin\theta_{2,i}\right]^T \tag{5}$$

As shown in Figure 2(b), $\boldsymbol{\eta}_i$ has a starting point at $\boldsymbol{R}_i$ ($\boldsymbol{O}$, $\boldsymbol{q}_i$ and $\boldsymbol{R}_i$ are on the same line). $\boldsymbol{R}_i$ is located on the plane π_i parallel to the tangent plane of the sphere at $\boldsymbol{q}_i$. We put pair of vectors as normal orthogonal bases $\{\boldsymbol{X}_i, \boldsymbol{Y}_i\}$ on π_i at $\boldsymbol{R}_i$.

$$\boldsymbol{X_i} = \begin{bmatrix} -\sin\theta_{1,i} \\ \cos\theta_{1,i} \\ 0 \end{bmatrix},\ \boldsymbol{Y_i} = \begin{bmatrix} -\sin\theta_{2,i}\cos\theta_{1,i} \\ -\sin\theta_{2,i}\sin\theta_{1,i} \\ \cos\theta_{2,i} \end{bmatrix} \tag{6}$$

Thus, $\boldsymbol{\eta_i}$ is linear combination of Eq. (6) and rotates counterclockwise with respect to ψ_i.

$$\boldsymbol{\eta_i} = \boldsymbol{X_i}\cos\psi_i + \boldsymbol{Y_i}\sin\psi_i \tag{7}$$

(B) ***Case of three-constraint driving rollers***

As shown in Figure 3, the locations between $l_1(v_1)$, $l_2(v_2)$, and $l_3(v_3)$, which depend on parameters v_1, v_2 and v_3, are used to determine the rotational axis of the sphere.

If a pair of v_1, v_2, and v_3 exists such that $l_1(v_1)$, $l_2(v_2)$, and $l_3(v_3)$ have common points, the endpoint of $\boldsymbol{\omega}$ can be uniquely determined using Eq. (4) (as $i = 1,2,3$) (Figure 3(a)). Based on Eq. (4) (as $i = 1,2,3$), $\boldsymbol{\omega}$ must be on $\mathbf{span}\{\boldsymbol{q_1},\boldsymbol{\eta_1}\} \cap \mathbf{span}\{\boldsymbol{q_2},\boldsymbol{\eta_2}\} \cap \mathbf{span}\{\boldsymbol{q_3},\boldsymbol{\eta_3}\}$. However, if a pair of v_1, v_2, and v_3 exists such that $l_1(v_1)$, $l_2(v_2)$, and $l_3(v_3)$ have common no points, slip can occur (Figure 3(b)). The sphere rotational axis is defined with respect to the arbitrary parameters v_1, v_2, and v_3.

2.2. *Calculation method of optimal point in sum of the squared distances*

In this section, we calculate the optimal point $\boldsymbol{Q_o} = (x_0, y_0, z_0)(\in \mathbb{R}^3)$, which is determined such that the sum of the squared distances between $\boldsymbol{Q} = (x,y,z)(\in \mathbb{R}^3)$ and $l_i(v_i)(i = 1,2,3)$ is minimized.

As shown in Figure 3(b), d_i denote the distances between $\boldsymbol{Q}$ and $l_i(v_i)$ in each line $l_i(v_i)$. it is represented as follows (See Appendix (A)):

$$d_i = \left\| \left(-\frac{v_i}{r}\right)\boldsymbol{\eta}_i + \frac{\langle \boldsymbol{P}_i, \boldsymbol{Q}\rangle}{r^2}\boldsymbol{P}_i - \boldsymbol{Q} \right\| \tag{8}$$

Therefore. Sum of the squared distances is represented as follow:

$$L(x,y,z) = {d_1}^2 + {d_2}^2 + {d_3}^2 \tag{9}$$

$(x,y,z) = (x_0, y_0, z_0)$ such that $L(x,y,z)$ is minimal value $A_{10} - {B_8}^2/4B_2$ is satisfy as following value (x_0, y_0, z_0) (See Appendix(B)).

$$z_0 = -\frac{C_9}{2C_3} \tag{10}$$

$$y_0 = \frac{B_5C_9 - 2C_3A_8}{4B_2C_3} \tag{11}$$

$$x_0 = \frac{1}{8A_1B_2C_3}(-A_4B_5C_9 + 2A_4B_8C_3 + 2A_6B_2C_9 - 4A_7B_2C_3) \tag{12}$$

Where

$$C_3 = B_3 - \frac{{B_5}^2}{4B_2}, C_9 = B_9 - \frac{B_5B_8}{2B_2}, C_{10} = B_{10} - \frac{{B_8}^2}{4B_2} \tag{13}$$

Where

$$B_2 = A_2 - \frac{{A_4}^2}{4A_1}, B_3 = A_3 - \frac{{A_6}^2}{4A_1}, B_5 = A_5 - \frac{A_4A_6}{2A_1}$$
$$B_8 = A_8 - \frac{A_4A_7}{2A_1}, B_9 = A_9 - \frac{A_6A_7}{2A_1}, B_{10} = A_{10} - \frac{{A_7}^2}{4A_1} \tag{14}$$

Where

$$\begin{aligned}
A_{10} &= L(0,0,0)\\
A_1 &= \frac{1}{2}\big(L(-1,0,0) + L(1,0,0) - 2L(0,0,0)\big)\\
A_2 &= \frac{1}{2}\big(L(0,-1,0) + L(0,1,0) - 2L(0,0,0)\big)\\
A_3 &= \frac{1}{2}\big(L(0,0,-1) + L(0,0,1) - 2L(0,0,0)\big)\\
A_7 &= \frac{1}{2}\big(L(1,0,0) - L(-1,0,0)\big)\\
A_8 &= \frac{1}{2}\big(L(0,1,0) - L(0,-1,0)\big)\\
A_9 &= \frac{1}{2}\big(L(0,0,1) - L(0,0,-1)\big)\\
A_4 &= \frac{1}{4}\big(L(1,1,0) - L(1,-1,0) - L(-1,1,0)\\
&\qquad + L(-1,-1,0)\big)\\
A_5 &= \frac{1}{4}\big(L(0,1,1) - L(0,1,-1) - L(0,-1,1)\\
&\qquad + L(0,-1,-1)\big)\\
A_6 &= \frac{1}{4}\big(L(1,0,1) - L(-1,0,1) - L(1,0,-1)\\
&\qquad + L(-1,0,-1)\big)
\end{aligned} \tag{15}$$

2.3 *Forward kinematics of sphere rotational motion*

We defined forward kinematics as input $v_i(i = 1,2,3)$ $\rightarrow$ output $\boldsymbol{V}$. The measured sphere robot direction angle from x-axis denotes φ and defined interval as $0° \le \varphi < 360°$. The sphere mobile velocity vector on the xy-plane denotes $\boldsymbol{V}$. Because that $\boldsymbol{\omega} = [\omega_x, \omega_y, \omega_z]^T$ is perpendicular to $\boldsymbol{V}$, The forward kinematics is represented as follows:

$$\|\boldsymbol{V}\| = r\sqrt{\omega_x^2 + \omega_y^2} \tag{16}$$

$$\varphi = \begin{cases} \cos^{-1}\left[\omega_y / \sqrt{\omega_x^2 + \omega_y^2}\right] & (\omega_x < 0) \\ 360° - \cos^{-1}\left[\omega_y / \sqrt{\omega_x^2 + \omega_y^2}\right] & (\omega_x \geq 0) \end{cases} \tag{17}$$

3. Simulation

This chapter presents the simulation results, including the trajectory of the endpoint of the sphere angler velocity vector $\boldsymbol{\omega}_k$, the sphere mobile velocity vector $\boldsymbol{V}_k$, and the slip vector $\boldsymbol{\zeta}_{i,k}$ and slip speed $\|\boldsymbol{\zeta}_k\|$ in *k-th* $(k = 1,2,3,4)$ roller arrangement patterns in the case in which a regular triangle ($\theta_{1,1}$, $\theta_{1,2}$, $\theta_{1,3}$)= (30°, 150°, 270°) and $\psi_i = 0°$ ($i = 1,2,3$) are fixed and $\theta_{2,i}$ is parameter as 0° ～30°. The patterns are set up by $\theta_{2,i}$ ($i = 1,2,3,4$) as follows: Pattern I ($k = 1, \theta_{2,i} = 0°$), Pattern II ($k = 2, \theta_{2,i} = 10°$), Pattern III ($k = 3, \theta_{2,i} = 20°$), Pattern IV ($k = 4, \theta_{2,i} = 30°$).

As input roller speed, we define function $v_1(\varphi) = \sin(\varphi + 240°)$, $v_2(\varphi) = \sin(\varphi + 120°)$ and $v_3(\varphi) = \sin\varphi$ such that output: $\|\boldsymbol{V}_1\| = 1$ [m/s].

As output, $\boldsymbol{\omega}_k$, $\boldsymbol{V}_k$, $\boldsymbol{\zeta}_{1,k}$, $\boldsymbol{\zeta}_{2,k}$, and $\boldsymbol{\zeta}_{3,k}$ ($k = 1,2,3,4$) were indicated, such as Pattern I [$k = 1$; green curve], Pattern II [$k = 2$; red curve], Pattern III [$k = 3$; blue curve], and Pattern IV [$k = 4$; violet curve] (Figure 4-9). They were calculated using Eqs. (10)-(12) and (16), respectively.

As shown in Figure 4, $\boldsymbol{\omega}_k$ ($k = 1,2,3,4$) draws circle trajectories and gets a small radius in turn.

As shown in Figure 5, $\boldsymbol{V}_k$ ($k = 1,2,3,4$) draws circle trajectories and gets a common center and small radius in turn.

As shown in Figure 6-8, $\boldsymbol{\zeta}_{i,1}$ is the only origin ($\boldsymbol{\zeta}_{i,1} = \boldsymbol{0}$) due to Pattern I (nonslip case), but $\boldsymbol{\zeta}_{i,2}$, $\boldsymbol{\zeta}_{i,3}$, and $\boldsymbol{\zeta}_{i,4}$ draw ellipsoid trajectories and get a large radius in turn. In this way, $\boldsymbol{V}_k$ (or $\boldsymbol{\omega}_k$) and $\boldsymbol{\zeta}_{i,k}$ are trade-off effects.

As shown in Figure 9, because Pattern I [$k = 1$: nonslip case], $\|\boldsymbol{\zeta}_{1,1}\|$, $\|\boldsymbol{\zeta}_{2,1}\|$, and $\|\boldsymbol{\zeta}_{3,1}\| = 0$ [m/s].

Three functions $\|\boldsymbol{\zeta}_{1,k}\|$, $\|\boldsymbol{\zeta}_{2,k}\|$, and $\|\boldsymbol{\zeta}_{3,k}\|$ with respect to φ are cyclical functions of $2\pi/3$.

$\|\boldsymbol{\zeta}_{1,k}\|$ $(k = 2,3,4)$ have minimal values of 0.03, 0.10, and 0.19 [m/s], respectively, when $\varphi = \pi/6, 7\pi/6$[rad]. $\|\boldsymbol{\zeta}_{1,k}\|(k = 2,3,4)$ have maximal values of 0.16, 0.30, and 0.40 [m/s], respectively, when $\varphi = 2\pi/3, 5\pi/3$.

$\|\boldsymbol{\zeta}_{2,k}\|(k = 2,3,4)$ has minimal values of 0.03, 0.10, and 0.19 [m/s], respectively, when $\varphi = 5\pi/6, 11\pi/6$.

$\|\boldsymbol{\zeta}_{2,k}\|(k = 2,3,4)$ has maximal values of 0.16, 0.30, and 0.40 [m/s], respectively, when $\varphi = \pi/3, 4\pi/3$.

$\|\boldsymbol{\zeta}_{3,k}\|(k = 2,3,4)$ has minimal values of 0.03, 0.10, and 0.19 [m/s], respectively, when $\varphi = \pi/2, 3\pi/2$, and $\|\boldsymbol{\zeta}_{3,k}\|(k = 2,3,4)$ has maximal values of 0.16, 0.30, and 0.40 [m/s], respectively, when $\varphi = 0, \pi, 2\pi$

In this way, the direction case in which slip speed is maximal is perpendicular to the direction case in which slip speed is minimal.

4. Conclusion

In this study, we considered the existence of an angular velocity vector of sphere driven by three rollers from the viewpoint of forward kinematics and demonstrated the trajectory of the endpoint of the angular velocity vector and slip velocity vector.

In the future research, we want to conduct the inverse kinematics and consider existence space for input rollers speed.

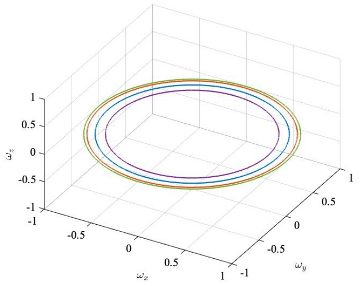

Figure 4 The trajectory of end point of angular velocity vector $\boldsymbol{\omega}_k (k = 1,2,3,4)$.

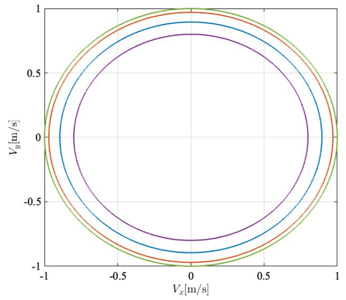

Figure 5 The trajectory of end point of angler velocity vector of the sphere $\boldsymbol{V}_k (k = 1,2,3,4)$.

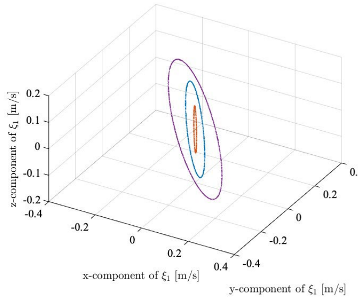

Figure 6 The trajectory of slip vector from sphere and roller $\boldsymbol{\zeta}_{1,k} (k = 1,2,3,4)$.

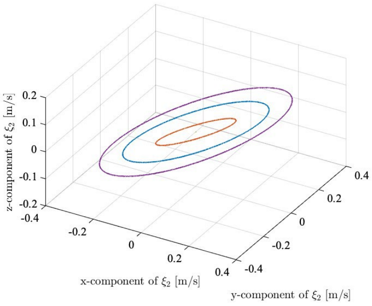

Figure 7 The trajectory of slip vector from sphere and roller $\boldsymbol{\zeta}_{2,k} (k = 1,2,3,4)$.

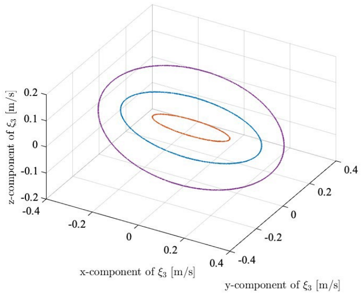

Figure 8 The trajectory of slip vector from sphere and roller $\boldsymbol{\zeta}_{3,k} (k = 1,2,3,4)$.

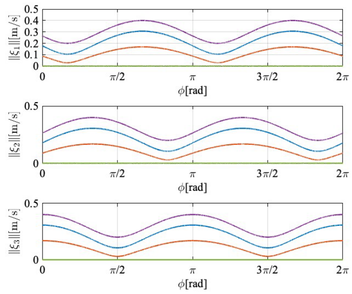

Figure 9 The slip speed of slip vector from sphere and roller $\|\boldsymbol{\zeta}_{1,k}\|$, $\|\boldsymbol{\zeta}_{2,k}\|$, $\|\boldsymbol{\zeta}_{3,k}\|$ $(k = 1,2,3,4)$.

Appendix

(A) Calculation of distance between $\boldsymbol{Q}$ and $\boldsymbol{l_i(v_i)}$

As shown in Figure 10, It is determined distance d_i such that $l_i(v_i) \perp \overrightarrow{\boldsymbol{QQ_i}}$ $(\boldsymbol{Q}_i \in l_i(v_i),\ \boldsymbol{Q} \in \boldsymbol{R}^3)$. Using Eq. (4) and inner product expand formula,

$$0 = \langle \boldsymbol{q_i}, \boldsymbol{Q}_i - \boldsymbol{Q} \rangle$$

$$= \left\langle \boldsymbol{q_i}, \left(-\frac{v_i}{r}\right)\boldsymbol{\eta}_i + \frac{t}{r}\boldsymbol{q}_i - \boldsymbol{Q} \right\rangle \quad \text{(A,1)}$$

$$= \left(-\frac{v_i}{r}\right)\langle \boldsymbol{q_i}, \boldsymbol{\eta}_i \rangle + \frac{t}{r}\langle \boldsymbol{q_i}, \boldsymbol{q}_i \rangle - \langle \boldsymbol{q_i}, \boldsymbol{Q} \rangle \quad \text{(A,2)}$$

From $\langle \boldsymbol{q_i}, \boldsymbol{\eta_i} \rangle = 0$ and $\langle \boldsymbol{q_i}, \boldsymbol{q_i} \rangle = r^2$, Eq. (A,2) can be simplified, and we obtain the value t that minimizes the distance between $\boldsymbol{Q}$ and $l_i(v_i)$ as follows:

$$\Leftrightarrow\ 0 = rt - \langle \boldsymbol{q_i}, \boldsymbol{Q} \rangle \Leftrightarrow t = \langle \boldsymbol{q_i}, \boldsymbol{Q} \rangle / r \quad \text{(A,3)}$$

Substituting $\overrightarrow{\boldsymbol{QH_i}} = \overrightarrow{\boldsymbol{OH_i}} - \overrightarrow{\boldsymbol{OQ}}$ with Eq. (A,3),

$$\overrightarrow{\boldsymbol{QH_i}} = \left(-\frac{v_i}{r}\right)\boldsymbol{\eta}_i + \frac{\langle \boldsymbol{q_i}, \boldsymbol{Q} \rangle}{r^2}\boldsymbol{q}_i - \boldsymbol{Q} \quad \text{(A,4)}$$

Therefore.

$$d_i = \left\| \left(-\frac{v_i}{r}\right)\boldsymbol{\eta}_i + \frac{\langle \boldsymbol{q_i}, \boldsymbol{Q} \rangle}{r^2}\boldsymbol{q}_i - \boldsymbol{Q} \right\| \quad \text{(A,5)}$$

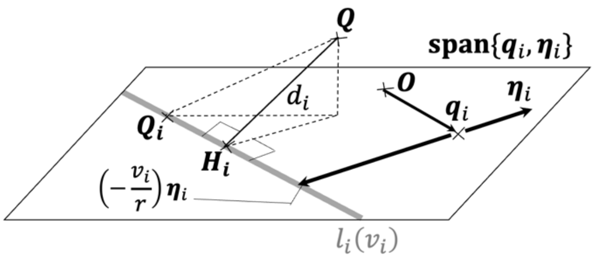

Figure 10 Distances between $\boldsymbol{Q}(\in \mathbb{R}^3)$ and $l_i(v_i)$

(B) Calculation of optimal point

First, based on the coefficients $A_1 \sim A_{10}$, $L_1(x, y, z)$ is represented as a quadratic equation with respect to, y and z as follows:

$$L_1(x, y, z) = A_1 x^2 + A_2 y^2 + A_3 z^2 \quad \text{(B,1)}$$

$$+ A_4 xy + A_5 yz + A_6 zx + A_7 x + A_8 y + A_9 z + A_{10}$$

Based on Eq. (B,1), the following homogeneous equation is conducted. By solving Eq. (B,2), We obtain A_1, A_2, A_3, A_7, A_8, A_9 and A_{10}.

$$\begin{aligned}
&L(0,0,0) = A_{10} \\
&L(1,0,0) = A_1 + A_7 + A_{10} \\
&L(-1,0,0) = A_1 - A_7 + A_{10} \\
&L(0,1,0) = A_2 - A_8 + A_{10} \\
&L(0,-1,0) = A_2 - A_8 + A_{10} \\
&L(0,0,1) = A_3 - A_9 + A_{10} \\
&L(0,0,-1) = A_3 - A_9 + A_{10}
\end{aligned} \tag{B,2}$$

Using Eq. (B,1), following homogeneous equation is conducted. By solving Eq. (B,3), we get A_4, A_5 and A_6.

$$\begin{aligned}
&L(1,1,0) = A_1 + A_2 + A_4 + A_7 + A_8 + A_{10} \\
&A_4 = L(1,1,0) - (A_1 + A_2 + A_7 + A_8 + A_{10}) \\
&A_5 = L(0,1,1) - (A_2 + A_3 + A_8 + A_9 + A_{10}) \\
&A_6 = L(1,0,1) - (A_1 + A_3 + A_7 + A_9 + A_{10})
\end{aligned} \tag{B,3}$$

At first, Eq. (B,1) is represented as follows by completing the square with respect to x.

$$L_2(x,y,z) = A_1(x + \frac{A_4 y + A_6 z + A_7}{2A_1})^2 \tag{B,4}$$

$$+B_2 y^2 + B_3 z^2 + B_5 yz + B_8 y + B_9 z + B_{10}$$

At second, Eq. (B,4) is represented as follows by completing the square with respect to y and z.

$$L_3(x,y,z) = A_1(x + \frac{A_4 y + A_6 z + A_7}{2A_1})^2 \tag{B,5}$$

$$+B_2(y + \frac{B_5 z + B_8}{2B_2})^2 + C_3(z + \frac{C_9}{2C_3})^2 + C_{10} - \frac{{C_9}^2}{4C_3}$$

$(x,y,z) = (x_0, y_0, z_0)$ such that $L_3(x,y,z)$ is minimal value $C_{10} - {B_8}^2/4B_2$ is satisfied as this linear equation with respect to x_0, y_0 and z_0.

$$\begin{cases} x_0 + \dfrac{A_4 y_0 + A_6 z_0 + A_7}{2A_1} = 0 \\ y_0 + \dfrac{B_5 z_0 + B_8}{2B_2} = 0 \\ z_0 + \dfrac{C_9}{2C_3} = 0 \end{cases} \tag{B,6}$$

Therefore. By solving Eq. (B,6), we get it.

Reference

[1] M. Wada, K. Kato, Kinematic Modeling and Simulation of Active-caster Robotic Drive with a Ball Transmission (ACROBAT-S), *2016 IEEE/RSJ International Conference on Intelligent Robots and Systems*. Daejeon, 2016-12-9/25, IEEE Robotics and Automation Society, 2016

[2] S. Ishida , H. Miyamoto, Holonomic Omnidirectional Vehicle with Ball Wheel Drive Mechanism, The Japan Society of Mechanical Engineers, Vol.78, No.790, pp.2162-2170, 2012.

[3] K. Kimura, K. Ishii, Y. Takemura, M. Yamamoto, Mathematical Modeling and motion analysis of the wheel based ball retaining mechanism, *SCIS & ISIS*, pp.4106-4111, 2016.

[4] K. Kimura, K. Ishii, The Spherical Robot Transfer Problem with Minimal Total Kinetic Energy, *Proceedings of International Conference on Artificial ALife and Robotics (ICAROB2021)*, pp.266-270, 2021.

[5] K. Kimura, K. Ishii, Efficiency Problem of Spherical Robot in Transfer Kinetic Energy, Journal of Robotics, Networking and Artificial Life, Vol.9, No.1 , pp.87-92, 2022.

[6] K.Kimura, K.Ishii, Roller's Kinetic Energy Efficency Problem on Upper Hemisphere , *2022 Joint 12th International Conference on Soft Computing and Intelligent Systems and 23rd International Symposium on Advanced Intelligent Systems (SCIS&ISIS)* 2022.

[7] K.Kimura, Y.Abematsu, H.Hirai, K.Ishii, Evaluation of Two Roller Arrangement on a Hemisphere by Kinetic Energy, Journal of Robotics, Networking and Artificial Life, Vol.9, No.3, pp.233-239, 2022.

[8] S. Chikushi, M. Kuwada, et al., Development of Next-Generation Soccer Robot"Musashi150"for RoboCup MSL, *30th Fussy System Symposium*, pp.624-627, 2014.

[9] Y.Yasohara, K.Shimizu et al., Development of Ball Handling Mechanism for RoboCup MSL, *30th Fussy System Symposium*, pp.616-617, 2014.

[10] R. Junkai, X. Chenggang, X. Junhao et al., A Control System for Active Ball Handling in the RoboCup Middle Size League, *Chinese Control and Decision Conference(CCDC.)*, 2016.

[11] K. Kimura, K. Ogata, K. Ishii, Novel Mathematical Modeling and Motion Analysis of a Sphere Considering Slipping, Journal of Robotics, Networking and Artificial Life, Vol.6, No.1, pp.27-32, 2019.

[12] K. Kimura, S. Chikushi, K. Ishii, Evaluation of the Roller Arrangements for the Ball-Dribbling Mechanisms Adopted by RoboCup Teams, Journal of Robotics, Networking and Artificial Life, Vol.6, No.3, pp.183-190, 2019.

[13] Y.C. Lee, D.V. Lee, J.H. Chung, S.A. Velinky, Control of a redundant, reconfigurable ball wheel drive mechanism for an omunidirectional platform,Robotica, Cambridge University Press, Vol.25, pp.385-395, 2007.

[14] M. Kumagai, T. Ochiai, Development of a Robot Balanced on a Ball – Application of Passive Motion to Transport, *2009 IEEE International Conference on Robotics and Automation*, pp.4106-4111, 2009.

[15] Y. Suzuki, H. Minakata, Developing Double Ball Balancing Robot- MATLAB Simulations of Ball Driving and Dynamics, *Proceedings of the 2016 JSME Conference on Robotics and Mechatronics*, Japan, 2A2-07a5 (1-4), 2016.

[16] T. Fujimura, M. Kumagai, Development of a Omnidirectional Vehicle with Two Spherical Wheels, *Proceedings of the 2017 JSME Conference on Robotics and Mechatronics*, Japan, 2A1-B09 (1-3), 2017.

[17] A. Weiss, R.G. Langlois, M.J.D. Hayes, The Effects of Dual-Row Omnidirectional Wheels on the kinematics of the Atlas Spherical Motion Platform, Mechanism and Machine Theory, Vol.44, No.2, pp.349-358, 2009.

Authors Introduction

Dr. Kenji Kimura

He is a Lecturer in Department of Control Engineering, National Institute of Technology, Matsue College, where he has been since 2022. He received his ME (mathematics) from Kyushu University in 2002 and received his Ph.D(Engineering) from Kyushu Institute of in 2020.His research interests spherical mobile robot .

Mr. Koki Ogata

He received his B.S., M.S., in Saga University, Japan, in 2021, 2023, respectively. He is an employee of DENSO CORPORATION, where he has been since 2023. His current research interests include sphere mobile robot kinematics, analytical dynamics.

Mr. Hiroyasu Hirai

He received his B.E., M.E., in Computer Science from Nippon Bunri University, Japan, in 2013, 2016, respectively. He is a 3rd year student in the doctoral program of the Kyushu Institute of Technology. He is an engineer of Garuda incorporated in 2016. His research interest includes autonomous robotics and machine learning (deep learning).

Mr. Takumi Ueda

He received his M.E., in Engineering from Kyusyu Institute of Technology, Japan, in 2017. He is a 3rd year student in the doctoral program of the Kyushu Institute of Technology. His research interest includes non-linear control by PID using database.

Dr. Kazuo Ishii

He is a Professor in the Kyushu Institute of Technology, where he has been since 1996. He received his Ph.D. degree in engineering from University of Tokyo, in 1996. His research interests span both ship marine engineering and Intelligent Mechanics. He holds five patents derived from his research.